

# Quasi-ballistic transport in HgTe quantum well nanostructures

V. Daumer,\* I. Golombek, M. Gbordzoe, E. G. Novik, V. Hock, C. R. Becker, H. Buhmann, and L. W. Molenkamp  
*Physikalisches Institut(EP 3), Universität Würzburg, Am Hubland, 97074 Würzburg, Germany*

(Dated: December 4, 2018)

The transport properties of micrometer scale structures fabricated from high mobility HgTe quantum wells have been investigated. A special photoresist and Ti masks were used, which allow for the fabrication of devices with characteristic dimensions down to  $0.45\ \mu\text{m}$ . Evidence that the transport properties are dominated by ballistic effects in these structures is presented. Monte Carlo simulations of semi-classical electron trajectories show good agreement with the experiment.

PACS numbers: 73.61.Ga, 73.23.Ad, 73.21.FG

The giant Zeeman effect and Rashba spin orbit (s-o) splitting<sup>1</sup> in magnetic 2DEG structures have recently aroused much interest due to their possible application in spintronics. These two effects are largest in the narrow gap II-VI semiconducting materials based on HgTe with which high mobility quantum well (QW) structures have been realized<sup>2</sup>. In addition it is possible to replace Hg substitutionally by isoelectronic magnetic atoms such as Mn, which enhances the effective g-factor, i. e.  $g^* \cong 50 - 60$ , whereas the sample mobilities are only weakly affected<sup>3</sup>. Therefore, HgTe QW structures offer interesting opportunities to study spin related transport effects. One goal is the exploration of the electronic spin behavior in nanostructures in which transport is dominated by ballistic effects. However, up to now ballistic transport has not been demonstrated in HgTe QW structures, mainly due to specific material properties that prevent the application of well known and established nano-structuring technologies used for Si and GaAs based structures. Here we report the first observations of ballistic transport in HgTe. In a cross shaped geometry with channel widths of  $0.45$  and  $1.0\ \mu\text{m}$  a non-local resistance signal is detected. The signal can be explained qualitatively and quantitatively by an approach based on the Landauer-Büttiker (LB) formula<sup>4</sup> and classical Monte Carlo (MC) simulations which consider the sample geometry only. The scattering time related to the transport mean free path is used as a fit parameter. The scattering time  $\tau$ , which is obtained from these simulations agrees well with that obtained from transport measurement on macroscopic Hall bar structures.

The  $n$ -type asymmetrically modulation doped QWs were epitaxially grown in a Riber 2300 MBE system on  $\text{Cd}_{0.96}\text{Zn}_{0.04}\text{Te}$  (001) substrates<sup>2,5</sup>. After an approximately  $60\ \text{nm}$  thick CdTe buffer layer, grown at  $315\ ^\circ\text{C}$ , the  $\text{CdI}_2$  modulation doped HgTe QWs were grown at  $180\ ^\circ\text{C}$ . The barriers consist of  $\text{Hg}_{0.3}\text{Cd}_{0.7}\text{Te}$  layers. The  $9\ \text{nm}$  thick iodine doped layer in the lower barrier is separated from the quantum well by a  $11\ \text{nm}$  spacer. The QW width is  $12\ \text{nm}$ . Sample parameters such as carrier concentration, mobility and Rashba s-o splitting were obtained from ac and dc measurements of a standard Hall bar in an  $^4\text{He}$  bath cryostat with magnetic fields perpendicular to the 2DEG up to  $7\ \text{T}$ . The Hall bar pattern was defined by optical lithography and wet chemical etching.

A carrier concentration of  $1.7 \times 10^{-16}\text{m}^{-2}$  and a carrier mobility of  $6.2\ \text{m}^2/(\text{Vs})$ , which corresponds to a Fermi wave vector  $k_F$  of  $3.27 \times 10^8\text{m}^{-1}$  and a inelastic mean free path  $l_i$  of  $1.3 \times 10^{-6}\text{m}$ , were obtained for the sample discussed here. Concluding from these results, it should be possible to observe ballistic transport effects in devices fabricated from this material with an active area of less than  $1\ \mu\text{m}^2$ . In standard nano-structuring lithographical processes, polymethylmethacrylate (PMMA) in conjunction with electron beam lithography is used to fabricate such structures. However, for epitaxially grown HgTe samples this is not possible due to the high bake-out temperature necessary for PMMA of about  $200\ ^\circ\text{C}$ . Temperatures exceeding  $100\ ^\circ\text{C}$  cause deterioration of the HgTe QW structures by interdiffusion of well and barrier materials. As an alternative, we have used the photoresist ARU 4060/3 (Allresist). This resist can be used not only for optical but also for electron beam lithographical pattern transfer. The advantage of this resist is the low bake-out temperature. For our samples a bake-out of  $2\ \text{min}$  at  $80\ ^\circ\text{C}$  was sufficient, which ensures that the sample structures remain unaffected. Samples were fabricated which exhibit a cross-shape geometry with lead widths of  $\sim 1.0\ \mu\text{m}$  (structure A) and  $\sim 0.45\ \mu\text{m}$  (structure B). A scanning electron microscope (SEM) image of structure B is shown in Fig. 1. These crosses have been written using an acceleration voltage of  $2.5\ \text{kV}$ . The positive resist was developed and Ti was evaporated onto the sample to serve as an etch mask for the subsequent wet chemical etching process. Ti masks must be used to avoid the strong under-etching that occurs with the use of a simple photoresist mask together with the etchant described below. Contact pads were fabricated in an optical lithography step with standard optical photoresist (Microresist ma-P215). Both optical and e-beam pattern were etched in a dilute solution of  $\text{Br}_2$  in ethylene glycol at room temperature for  $30\ \text{s}$ . After etching about  $150\ \text{nm}$  into the CdTe buffer layer, the resist and the Ti mask were removed with acetone and a  $2:1\ \text{H}_2\text{O}:\text{HF}(50\%)$  solution for  $10\ \text{s}$ , respectively. Ohmic contacts were fabricated by thermal bonding with indium. Quasi-dc, low frequency ( $13\ \text{Hz}$ ) ac measurements with an excitation voltage of  $150\ \mu\text{V}$  were carried out using lock-in techniques. Various contact combinations have been used to characterize the sample after the etching process. In the

Hall geometry (I: 1→3, V: 2→4, c.f. Fig. 1) the carrier concentration was found to be the same as that of macroscopic samples and therefore shows clearly, that the sample properties have not been changed by the fabrication process.

In order to demonstrate that the transport properties are dominated by ballistic effects we have performed non-local transport measurements in different contact arrangements, which previously have been successfully demonstrated in high mobility GaAs nano-structures<sup>6,7</sup>. One of the most prominent effects is in the non-local *bend* resistance (NLR). This signal is measured by passing current through contacts 1 and 2, while the voltage is measured between contacts 3 and 4 (see Fig. 1). The bend resistance is obtained simply by dividing the voltage  $V_{3,4}$  by the injected current. If the transport were dominated by diffusive scattering, no voltage signal would be expected to appear between contacts 3 and 4 in this geometry, whereas in the ballistic regime, electrons injected from contact 1 into the cross reach the opposite channel before they are scattered. This leads to charge accumulation at contact area 3 and thus to the NLR signal. Applying a small magnetic field perpendicular to the 2DEG plane deflects the ballistic electrons and the voltage signal between 3 and 4 decreases. The results are shown for a 1.0 and 0.45  $\mu\text{m}$  cross in Fig. 2. The NLR signal is indeed observed, which is direct evidence of ballistic transport in this device. As expected, the signal exhibits a pronounced maximum around  $B = 0$ . With an applied field the signal decreases, exhibiting a large dip with a negative NLR signal before it approaches zero in the high field range ( $B > 2\text{T}$ ). This behavior of the NLR signal can be qualitatively understood by applying the LB formalism. In our geometry the resulting NLR is derived to be as follows:

$$(R_{12,34}) = \frac{V_c}{I_i} = \frac{h}{2e^2} \frac{T^2 - t_r t_l}{(t_r + t_l)(2T^2 + 2(t_r + t_l)T + t_r^2 + t_l^2)} \quad (1)$$

where in our notation,  $T$  is the transmission probability of electrons from contact 1 in contact 3, and  $t_l$  and  $t_r$  are the transmission probabilities from contact 1 to contacts 2 and 4 respectively. Comparing this result with the data presented in Fig. 2, one can see that at zero magnetic field the NLR signal is dominated by electrons that travel ballistically from contact 1 to 3 ( $T^2$ , Eq.(1)). This signal is reduced by electrons which reach either the left or right contact ( $t_r, t_l$ , Eq.(1)). At zero magnetic field this corresponds to electrons that are either injected outside the acceptance angle of contact 3 or are scattered by unintentional impurities. In a magnetic field the electrons are deflected due to the Lorentz force either toward the left or the right contact, which implies that the NLR should decrease and approach zero, i.e.,  $T = 0$  and, either  $t_l = 0$  or  $t_r = 0$ . However, due to the boundary scattering processes mentioned above, an intermediate field regime exists where the signal becomes negative. In this regime the so called rebound trajectories<sup>7</sup> may cause the product  $t_l t_r$  to exceed  $T^2$ . Enlarging the B field fur-

ther will *guide* all electrons to only one contact ( $T^2 \rightarrow 0$  and, either  $t_r \rightarrow 0$  or  $t_l \rightarrow 0$ ) and the NLR becomes zero. In the inset of Fig. 2 one can see that in the regime where  $R_{12,34}$  is expected to approach zero, Shubnikov-de Haas oscillations, which are not included in Eq. 1, are superimposed on the signal. However, the ratio of the absolute magnitude of the positive signal at  $B = 0$  and the largest negative value is rather small compared to the published results for high mobility GaAs structures<sup>6,7,8</sup>. The main reason for this difference is the comparatively short mean free path, which is of the order of the device dimensions in the present case. Therefore, it is plausible that impurity scattering in the cross area increases the transmission probability to contacts 2 and 4, leading to a reduction in the NLR signal at zero magnetic field. This effect is also observed, when the device size is increased; the NLR signal for the 1.0  $\mu\text{m}$  structure is much smaller than that for the 0.45  $\mu\text{m}$  structure, as shown in Fig. 2. In a first approximation the ratio of the signal for these two structures can be used to estimate the carrier mean free path in the cross area. The signal is proportional to the number of electrons that reach contact 3 ballistically ( $\propto \exp -(L/l_i)$ ) reduced by those electrons that are scattered into the contacts 2 and 4 ( $\propto 1 - \exp -(L/l_i)$ ). Evaluating the values deduced from Fig. 2 a  $l_i \approx 1.2 \mu\text{m}$  is obtained which is in good agreement with the average mean-free path for the macroscopic sample.

In order to put these considerations on a more quantitative basis we have used a MC simulation of the classical electron trajectories in which electrons with an arbitrary velocity distribution are injected through contact 1 into the cross. In this model the electrons are then specularly reflected at the sample boundaries. The electrons that reach the individual contacts are counted. This number is proportional to the corresponding transmission probability<sup>7,9</sup>. Quantitatively, the experimental results can not be fully explained by purely ballistic transport and boundary scattering. From the measurements (Fig. 2) one observes that the signal exhibits additional fine structure which is not induced by electronic noise. This fine structure is fully reproducible and stable in time provided the sample is kept at low temperatures. We identify the fine structure as universal conductance fluctuation (UCF) electronic interference effects due to the random distribution of scatterers within the cross area. Evidently, MC simulations of classical electron trajectories are not appropriate to simulate these interference effects. However, the overall line shape and amplitude of the NLR signal can be reproduced by MC calculations when inelastic scattering is considered, i.e. the ballistic propagation is altered randomly for electrons that dwell longer than the inelastic scattering time  $\tau$  in the cross area. Fig. 3 shows the resulting NLR curve. For a scattering time of  $\tau = 1.1 \times 10^{-12}$  s a good agreement with the experimental data is obtained. This value implies a mean free path of  $\approx 0.9 \mu\text{m}$  and agrees well with the  $\tau = 1.6 \times 10^{-12}$  s ( $\Rightarrow l_i = 1.3 \mu\text{m}$ ), obtained from the macroscopic transport measurements and the value

deduced from the peak height ( $l_i = 1.2 \mu\text{m}$ ) discussed above. The inelastic scattering is likely due to remote ionized impurity scattering. These results demonstrate that for the given device dimensions, electrons either reach the contacts ballistically or are scattered inelastically. This implies that transport in these structures is in the transition regime between ballistic and diffusive transport, which is usually referred to as quasi-ballistic transport.

In conclusion, we have presented the first evidence of quasi-ballistic transport in high mobility HgTe QW

nano-structures which are fabricated with a technology that overcomes the specific problems of Hg containing devices. Furthermore, a quantitative analysis of the non-local resistance measurements revealed that the actual HgTe QW nanostructure samples allow for a detailed study of the transition from a diffusive to a local ballistic transport regime.

The financial support of the Deutsche Forschungsgemeinschaft (SFB 410), the Alexander von Humboldt Stiftung, and the DARPA SPINS program is gratefully acknowledged.

---

\* Electronic address: daumer@physik.uni-wuerzburg.de

<sup>1</sup> E.I. Rashba, *Fiz. Tverd. Tela* **2**, 1224 (1960) [ *Sov. Phys. Solid State* **2**, 1109 (1960)]; Yu. A. Bychkov and E.I Rashba, *Pis'ma Zh. Eksp. Teor. Fiz.* **39**, 66 (1984) [*JETP Lett.* **39**, 78 (1984)].

<sup>2</sup> X. C. Zhang, A. Pfeuffer-Jeschke, K. Ortner, V. Hock, H. Buhmann, C. R. Becker, and G. Landwehr, *Phys. Rev. B* **63** (24), 245305 (2001).

<sup>3</sup> X. C. Zhang, K. Ortner, A. Pfeuffer-Jeschke, C. R. Becker, R. Winkler, and G. Landwehr, to be published.

<sup>4</sup> M. Büttiker, *IBM J. Res. Dev.* **32**, 317 (1988).

<sup>5</sup> F. Goschenhofer, J. Gerschütz, A. Pfeuffer-Jeschke, R. Helmig, C. R. Becker, and G. Landwehr, *J. Elec. Mat.* **27**, 532 (1998).

<sup>6</sup> L.W. Molenkamp, A.A.M. Staring, C.W.J. Beenakker, R. Eppenga, C.E. Timmering, J.G. Williamson, C.J.P.M. Harman, and C.T. Foxon, *Phys. Rev. B* **41**, 1274 (1990).

<sup>7</sup> A.S.D. Heindrichs, H. Buhmann, S.F. Godijn, and L.W. Molenkamp, *Phys. Rev. B* **57**, 3961 (1998).

<sup>8</sup> G. Timp, in *Semiconductor and Semimetals* Vol. 35, edited by M. Reed, Academic Press, London (1992).

<sup>9</sup> C.W.J. Beenakker and H. van Houten, in *Electronic Properties of Multilayers and Low-Dimensional Semiconductor Structures*, edited by J.M. Chamberlain (Plenum, New York, 1990).

FIG. 1: SEM photograph of a cross with  $0.45 \mu\text{m}$  wide leads.

FIG. 2: Non-local resistance signal (NLR) for structures with lead widths of  $1.0 \mu\text{m}$  (structure A) and  $0.45 \mu\text{m}$  (structure B). The inset shows the NLR of the smaller device for an extended magnetic field range.

FIG. 3: Experimental data for a  $0.45 \mu\text{m}$  device together with the Monte Carlo simulation result (smooth curve) for a scattering time of  $\tau = 1.1 \times 10^{-12}$  s.

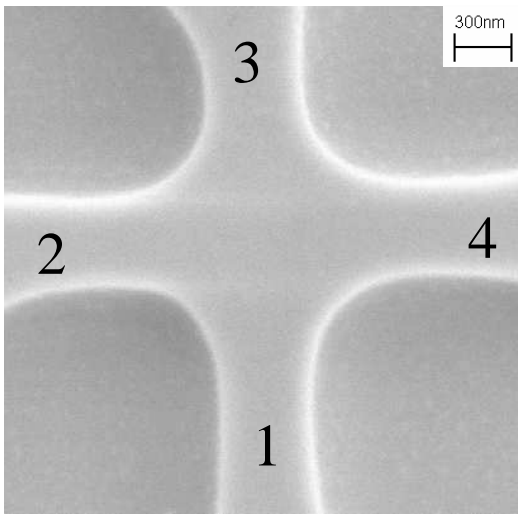


FIG. 1: SEM photograph of a cross with  $0.45 \mu\text{m}$  wide leads.

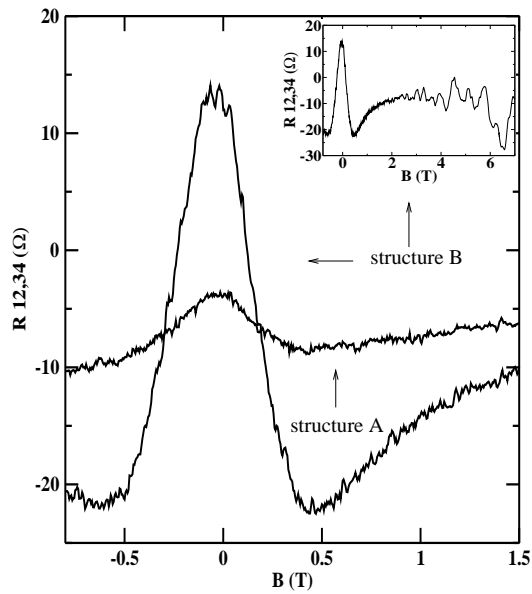


FIG. 2: Non-local resistance signal (NLR) for structures with lead widths of  $1.0 \mu\text{m}$  (structure A) and  $0.45 \mu\text{m}$  (structure B). The inset shows the NLR of the smaller device for an extended magnetic field range.

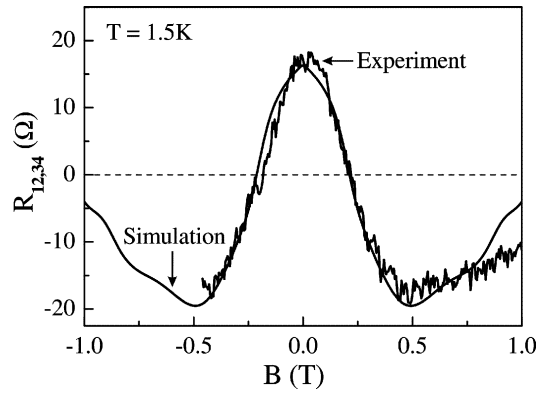


FIG. 3: Experimental data for a  $0.45\ \mu\text{m}$  device together with the Monte Carlo simulation result (smooth curve) for a scattering time of  $\tau = 1.1 \times 10^{-12}$  s.